Original Article | Musculoskeletal Imaging

eISSN 2005-8330
https://doi.org/10.3348/kjr.2018.0517
Korean J Radiol 2019;20(3):469-478

Korean Journal of Radiology
KJR

Cervical Spine CT Using Spectral Shaping: Can It Be a Solution to Overcome Artifacts in the Lower Cervical Spinal Region?

Su Min Lee, MD[1], Hye Jung Choo, MD, PhD[1], Sun Joo Lee, MD, PhD[1], Sung-Kwan Kim, MD[1], In Sook Lee, MD, PhD[2], Dong Wook Kim, MD, PhD[1], Jin Wook Baek, MD[1], Young Jin Heo, MD[1]

[1]Department of Radiology, Inje University Busan Paik Hospital, Busan, Korea; [2]Department of Radiology, Biomedical Research Institute, Pusan National University Hospital, Busan, Korea

Objective: To investigate the image quality, radiation dose, and intermodality agreement of cervical spine CT using spectral shaping at 140 kVp by a tin filter (Sn140-kVp) in comparison with those of conventional CT at 120 kVp.
Materials and Methods: Patients who had undergone cervical spine CT with Sn140-kVp (n = 58) and conventional 120 kVp (n = 49) were included. Qualitative image quality was analyzed using a 5-point Likert scale. Quantitative image quality was assessed by measuring the noise and attenuation within the central spinal canals at C3/4, C6/7, and C7/T1 levels. Radiation doses received by patients were estimated. The intermodality agreement for disc morphology between CT and MRI was assessed at C3/4, C5/6, C6/7, and C7/T1 levels in 75 patients who had undergone cervical spine MRI as well as CT.
Results: Qualitative image quality was significantly superior in Sn140-kVp scans than in the conventional scans ($p < 0.001$). At C7/T1 level, the noise was significantly lower and the decrease in attenuation was significantly less in Sn140-kVp scans, than in the conventional scans ($p < 0.001$). Radiation doses were significantly reduced in Sn140-kVp scans by 50% (effective dose: 1.0 ± 0.1 mSv vs. 2.0 ± 0.4 mSv; $p < 0.001$). Intermodality agreement in the lower cervical spine region tended to be better in Sn140-kVp acquisitions than in the conventional acquisitions.
Conclusion: Cervical spine CT using Sn140-kVp improves image quality of the lower cervical region without increasing the radiation dose. Thus, this protocol can be helpful to overcome the artifacts in the lower cervical spine CT images.
Keywords: *Cervical spine; Multidetector computed tomography; Spectral; Metal artifact*

INTRODUCTION

Cervical spine CT is widely used in the evaluation of cervical spinal abnormalities. American College of Radiology has recommended cervical spine CT as a primary imaging modality in suspected spine trauma because of its high sensitivity and specificity to detect fractures (1). Cervical spine CT has been suggested as an alternative modality to MRI even for the diagnosis of a herniated disc or spinal stenosis due to shorter scan time and cost-effectiveness (2). However, the diagnosis of lesions at the lower cervical region on CT is challenging due to the presence of streaks and dark bands, which are explained as photon starvation or beam-hardening artifacts generated by the shoulder girdles (3, 4). The diagnosis of a disc pathology or spinal stenosis is more problematic because the artifacts are usually more severe in the central spinal canals. A simple method to remove the artifacts is by using a high tube current or voltage. However, this is accompanied by a radiation dose penalty. Although there have been trials and technical developments such as shoulder reposition and automatic tube current modulation to solve this issue (5, 6), the dark-

Received August 3, 2018; accepted after revision November 3, 2018.
This study was supported by the DongKook Life Science. Co., Ltd., Republic of Korea.
Corresponding author: Hye Jung Choo, MD, PhD, Department of Radiology, Inje University Busan Paik Hospital, 75 Bokji-ro, Busanjin-gu, Busan 47392, Korea.
• Tel: (8251) 890-6549 • Fax: (8251) 896-1085
• E-mail: hyejungchoo@gmail.com
This is an Open Access article distributed under the terms of the Creative Commons Attribution Non-Commercial License (https://creativecommons.org/licenses/by-nc/4.0) which permits unrestricted non-commercial use, distribution, and reproduction in any medium, provided the original work is properly cited.

Copyright © 2019 The Korean Society of Radiology

band and streak artifacts in the lower cervical area on CT still remain problematic.

Recently, "spectral shaping" of photon energy spectrum by a tin filter has been introduced. The tin filter, which is added to the standard aluminum bowtie filter between X-ray tube and the patients, absorbs low-energy photons that contribute less to the image quality but increase the radiation exposure to patients, and results in an increase in the mean photon energy of the applied radiation (7). Several latest studies demonstrated that the spectral shaping with a tin filter allowed for reduction of the radiation dose, while maintaining the image quality (8-13). Thus, we hypothesized that a high-energy tube voltage with spectral shaping by a tin filter might make it possible to overcome the artifacts in the lower cervical spine area in CT without an increase in the radiation dose.

Therefore, the purpose of this study was to investigate the image quality, radiation dose, and intermodality agreement of cervical spine CT using spectral shaping at 140 kVp by a tin filter (Sn140-kVp) in comparison with those of the conventional cervical spine CT at 120 kVp (120-kVp).

MATERIALS AND METHODS

This retrospective study was approved and informed consent was waived by the Institutional Review Board.

Study Population

This study enrolled 136 patients who had undergone non-enhanced cervical spine CT with Sn140-kVp protocol and 105 patients who had undergone conventional 120-kVp cervical spine CT between January 2017 and September 2017 in our institution. Among them, the patients with metal devices in the cervical spines (n = 82), fracture of the cervical spine (n = 38), severe spinal stenosis (n = 11), and infection of the cervical spine (n = 3) were excluded. Finally, 58 patients (31 men and 27 women; mean age, 58 years; age range, 28–83 years) who had undergone CT with Sn140-kVp CT were selected as the study group and 49 (25 men and 24 women; mean age, 57 years; age range, 25–83 years) with conventional CT as the control group. Thirty-seven patients in the study group (23 men, 14 women; mean age, 61 years) and 38 in the control group (21 men, 17 women; mean age, 57 years) underwent cervical spine MRI within three months before or after the cervical spine CT (median interval, 7 days; interval range, 0–90 days).

CT and MRI Acquisitions

A third-generation dual-source CT (DSCT) (Somatom Drive, Siemens Healthcare, Forchheim, Germany) was utilized for the Sn140-kVp protocol. This protocol included a dedicated tin filter mounted in front of the X-ray tube, which resulted in the spectral shaping of the polychromatic X-ray and increased the mean photon energy by shutting down the low levels of energy. Conventional 120-kVp CT was performed using single-source CT (Somatom Definition AS, Siemens Healthcare). Automatic tube current modulation (CareDose 4D, Siemens Healthcare) was activated in both protocols with a reference tube current-time product of 280 mAs for Sn140-kVp and 275 mAs for 120-kVp. All the images were reformatted into axial and sagittal planes with a 2-mm thickness and the axial planes were reformatted parallel to the orientation of each intervertebral disc. The parameters for each protocol are summarized in Table 1.

The cervical spine MRI was obtained by a 3T MR system (Magnetom Skyra, Siemens Healthcare, Erlangen, Germany) and a 64-channel head-neck coil. The parameters for the cervical spine MRI are summarized in Table 2.

Table 1. Parameters for Cervical Spine CT

Parameter	Sn140-kVp	120-kVp
Tube voltage (kVp)	140	120
Reference tube current-time products (mAs)	280	275
Detector configuration (mm)	128 x 0.6	128 x 0.6
Pitch	0.6	0.6
Rotation time (sec)	1	1
Field of view (mm)	120 x 120	120 x 120
Reconstruction algorithm	Filtered back projection soft-tissue kernel	Filtered back projection soft-tissue kernel
Reformatted section thickness (mm)	2	2
Reformatted section increment (mm)	2	2

Sn140-kVp = cervical spine CT using spectral shaping at 140 kVp by tin filter, 120-kVp = cervical spine CT at 120 kVp

https://doi.org/10.3348/kjr.2018.0517

Korean Journal of Radiology
KJR

Image Analysis

Three radiologists (readers A and B with 11-year and 5-year experiences in musculoskeletal radiology, respectively; reader C with 3-year experience in clinical radiology) blinded to the CT protocols and patients' information, reviewed the images.

Body Habitus

For an arbitrary estimation of the body habitus of the patients, the level and right-to-left (RL) diameter of the shoulder girdles and the anterior-to-posterior (AP) diameter of the neck were evaluated by the reader C because the body habitus could affect the CT image quality and radiation dose. The level of the shoulder girdle was recorded as the order of the vertebral body superimposed by the upper margin of the humeral head on the lateral CT scout view. The RL diameter of the shoulder girdle was measured at the level of the superior end of the humerus on an AP CT scout view. The AP diameter of the neck was measured parallel to the intervertebral disc at C6/7 on the lateral CT scout view (14).

Image Quality

The image quality was analyzed using both qualitative and quantitative methods. For qualitative image analysis, the three readers independently scored the image quality on the sagittal image plane by using a 5-point Likert scale (1, non-diagnostic; 2, limited diagnostic value with substantial image noise and artifacts; 3, diagnostic, sufficient image quality; 4, diagnostic, good image quality with mild image noise and artifacts; 5, diagnostic, excellent image quality with absent or subtle noise and artifacts) focusing on the inside of the central spinal canal in the lower cervical spinal region including the cervicothoracic junction (13) (Fig. 1). Before the individual review, the readers trained themselves using a training dataset of 10 cases outside the study cohort, which was prepared by the study coordinator. During the

Table 2. Parameters for Cervical Spine MRI

Parameter	Sagittal T1-Weighted Fast Spin-Echo	Axial T1-Weighted Fast Spin-Echo	Sagittal T2-Weighted Fast Spin-Echo	Axial T2-Weighted Fast Spin-Echo
Repetition time (msec)	440	600	4000	2950
Echo time (msec)	11	13	62	108
Matrix size	512 x 358	320 x 256	512 x 269	384 x 269
Slice thickness (mm)	3	3	4	4
Interslice gap (mm)	0.3	0.3	0.5	0.5
No. of signals acquired	2	2	4	2
Imaging time	2 min 41 sec	2 min 33 sec	3 min 16 sec	2 min 17 sec

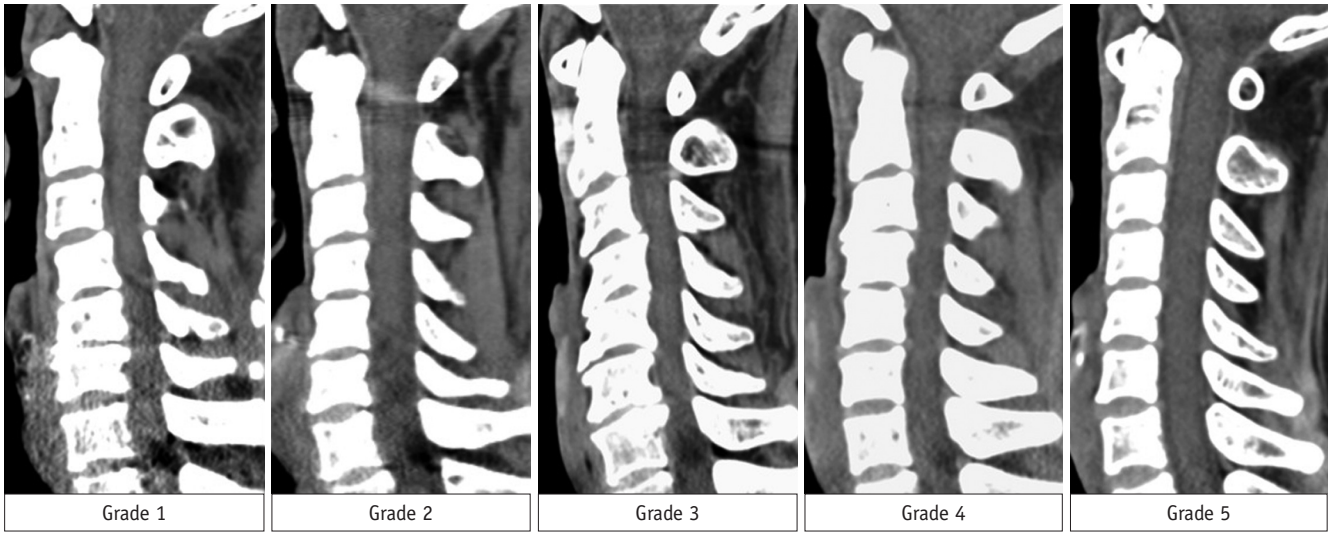

Fig. 1. Grading system for analysis of qualitative image quality. Qualitative image quality was scored on sagittal image plane by using 5-point Likert scale (1, non-diagnostic; 2, limited diagnostic value with substantial image noise and artifacts; 3, diagnostic, sufficient image quality; 4, diagnostic, good image quality with mild image noise and artifacts; 5, diagnostic, excellent image quality with absent or subtle noise and artifacts) focusing on inside of central spinal canal in lower cervical spinal region including cervicothoracic junction.

https://doi.org/10.3348/kjr.2018.0517

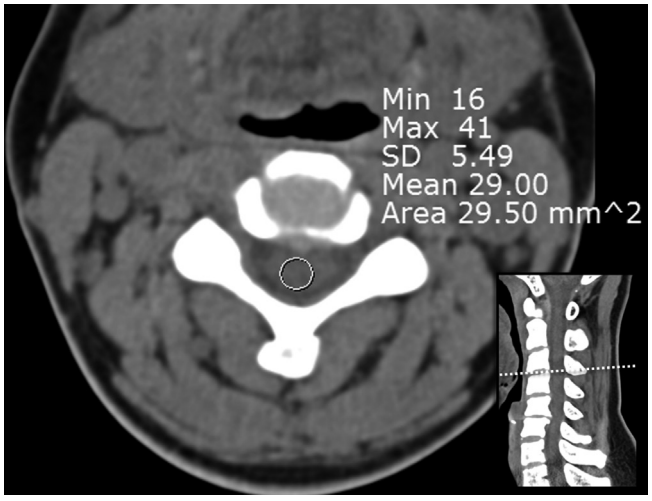

Fig. 2. Measurement for analysis of quantitative image quality. About 30-mm^2 circular region of interest was placing in center of central spinal canal on axial CT image of intervertebral disc level. To minimize bias, measurements were performed at three sequential slices and averaged. SD = standard deviation

qualitative analysis, all images were displayed with a window level/width set of 45/350 Hounsfield units (HUs).

For quantitative analysis, the CT attenuation values and noises (standard deviation [SD] of the attenuation values) inside the central spinal canals were measured at the intervertebral disc levels of C3/4, C6/7, and C7/T1 by the reader A. C3/4 was included for obtaining the baseline data that were not affected by the shoulder girdles. For measurements, an approximately 30-mm^2 circular region of interest (ROI) was placed in the center of the central spinal canal on the axial image plane (Fig. 2). Additionally, for the evaluation of signal-to-noise ratio (SNR) and contrast-to-noise ratio (CNR) of the bones, an approximately 60-mm^2 circular ROI was placed in the center of the bodies of the C3, C6, and C7 vertebrae on the mid-sagittal plane. The SNR of the bones was calculated by dividing the average of attenuation values by the SD in the ROI. The CNR between the vertebral body and the central spinal canal was calculated using the following equation (15):

$$|(\text{Attenuation value}_{\text{bone}} - \text{Attenuation value}_{\text{central canal}})| / \sqrt{(\text{SD}_{\text{bone}}^2 + \text{SD}_{\text{central canal}}^2)}$$

To minimize the bias, all measurements were performed at the three sequential slices and averaged.

Intermodality Agreement for Disc Morphology between CT and MRI

On the axial and sagittal planes of the cervical spine CT and MRI, the disc morphology was determined into normal disc, bulging, protrusion, and extrusion at the levels of C3/4, C5/6, C6/7, and C7/T1 by two radiologists (readers A and B) in consensus (16). The two sets of CT and MRI were reviewed separately.

Radiation Dose

The radiation exposure to patients was estimated by volume CT dose index ($CTDI_{vol}$), dose length product (DLP), and effective dose. The $CTDI_{vol}$ and DLP were automatically provided by the scanner systems. The effective radiation dose was calculated by multiplying the DLP by the appropriate conversion coefficients, 0.0052 mSv x mGy^{-1} x cm^{-1} for Sn140-kVp protocol (adult's neck region in 140 kVp) and 0.0051 mSv x mGy^{-1} x cm^{-1} for the conventional 120-kVp protocol (adult's neck region in 120 kVp) (17).

Statistical Analysis

The normality of the continuous variables was tested by using the Kolmogorov-Smirnov test. The normally distributed variables (age of the patients and diameters of the shoulders and necks) were reported as means ± SD and compared using the Student's *t* test. The non-normally distributed continuous variables (noise, attenuation, SNR and CNR of the bone, $CTDI_{vol}$, DLP, and effective radiation dose) and the ordinal variable (qualitative image quality) were reported as medians ± interquartile ranges and analyzed using the Mann-Whitney U test. Fisher's exact test was used for the comparison of the categorical variables (sex and the shoulder level). The relationship between CT radiation doses and diameters of the shoulders and necks was evaluated using the Pearson correlation test.

Interobserver agreement for the qualitative image quality among the three readers was assessed using the weighted kappa (κ). Intermodality agreement of the disc morphology between CT and MRI were evaluated in terms of κ. The degree of agreement (κ value) was categorized as follows: < 0, poor; 0–0.20, slight agreement; 0.21–0.40, fair agreement; 0.41–0.60, moderate agreement; 0.61–0.80, substantial agreement; and 0.81–1, almost perfect agreement (18).

All statistical analyses were performed using SPSS (SPSS Statistics version 24; IBM Corp., Armonk, NY, USA) and MedCalc (MedCalc Software bvba version 17.11.5, MedCalc Corp., Ostend, Belgium). A two-sided *p* value of less than 0.05 was considered to indicate a statistically significant difference.

https://doi.org/10.3348/kjr.2018.0517

Korean Journal of Radiology
KJR

Table 3. Demographics and Body Habitus of Patients

	Sn140-kVp (n = 58)	120-kVp (n = 49)	*P*
Demographics			
Age (years)*	58 ± 14	57 ± 14	0.557
Sex†			0.700
Male	31 (53%)	25 (51%)	
Female	27 (47%)	24 (49%)	
Body habitus			
Shoulder level†			0.165
C6	1 (2%)	2 (4%)	
C7	23 (40%)	16 (32%)	
T1	29 (50%)	25 (51%)	
T2	5 (9%)	6 (12%)	
Shoulder RL diameter (mm)*	396.0 ± 33.2	401.5 ± 32.6	0.419
Neck AP diameter (mm)*	121.6 ± 13.1	122.9 ± 13.4	0.608

*Data are means ± standard deviations, †Data are numbers (percentages). AP = anterior-to-posterior, RL = right-to-left

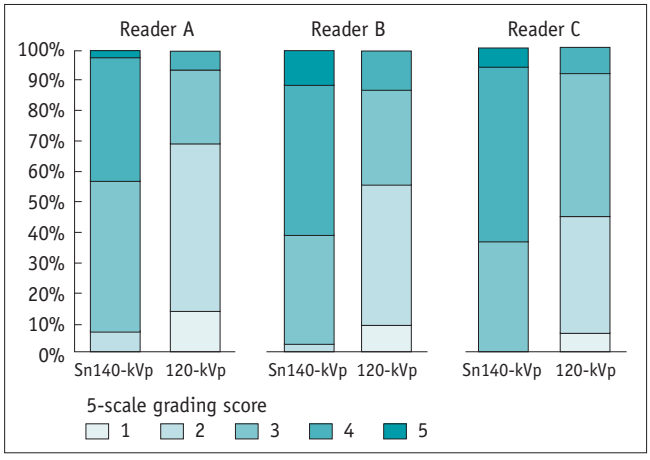

Fig. 3. Column chart for analysis of qualitative image quality.
Three readers determined qualitative image quality by using 5-point Likert scale (1, non-diagnostic; 2, limited diagnostic value with substantial image noise and artifacts; 3, diagnostic, sufficient image quality; 4, diagnostic, good image quality; 5, diagnostic, excellent image quality). Grading scores are statistically significant higher in cervical spinal CT with Sn140-kVp than 120-kVp by all three readers. Sn140-kVp = cervical spine CT using spectral shaping at 140 kVp by a tin filter, 120-kVp = cervical spine CT at 120 kVp

RESULTS

Demographics and Body Habitus

Age and sex of patients, diameters and level of the shoulder girdles, and diameter of the neck were not significantly different between the study and control groups. C7 and T1 were the common levels of the shoulder girdles in both groups (Table 3). In patients who underwent both cervical spine MRI and CT within a 3-month interval, these demographics and body habitus were not significantly different between the two subgroups.

Image Quality

The scores for the qualitative image quality by all three readers were significantly higher in Sn140-kVp acquisitions than in the conventional acquisitions (median scores: 4 by all readers in Sn140-kVp scans, 3 by readers B and C, and 2 by reader C in conventional scans; $p < 0.001$ for all readers) suggesting that the qualitative image quality of CT with Sn140-kVp acquisitions was significantly superior to that of conventional 120-kVp CT acquisitions (Figs. 3, 4). The scores showed moderate interobserver agreement ($\kappa = 0.693$ between readers A and B; 0.695 between readers A and C; 0.605 between readers B and C).

The quantitative image quality was analyzed at the three intervertebral disc levels (Table 4). The attenuation values in the central spinal canals were gradually decreasing, and the noises were gradually increasing from C3/4 to C7/T1 levels in both groups (Figs. 5, 6). However, the noises at C7/T1 level were significantly lower in Sn140-kVp scans than in the conventional 120-kVp scans ($p < 0.001$). The decrease in the attenuation values at C7/T1 level was also significantly less in Sn140-kVp scans than that in the conventional scans, although the median attenuation value for Sn140-kVp scan was less than 0 HU. The noises at C6/7 as well as C3/4 levels were not significantly different between the two groups as these levels were not severely affected by the shoulder girdles, which were mainly at C7 or T1 level in the included patients. The attenuation values at C6/7 level were not significantly different between the two groups whereas those at C3/4 level were significantly lower in Sn140-kV scans than in the conventional scans.

The SNR and CNR of the bones were not significantly

https://doi.org/10.3348/kjr.2018.0517

different between the Sn140-kV scans and conventional 120-kVp scans in all C3, C6, and C7 levels (Table 5).

Intermodality Agreement for Disc Morphology between CT and MRI

The disc morphology showed almost perfect agreement in

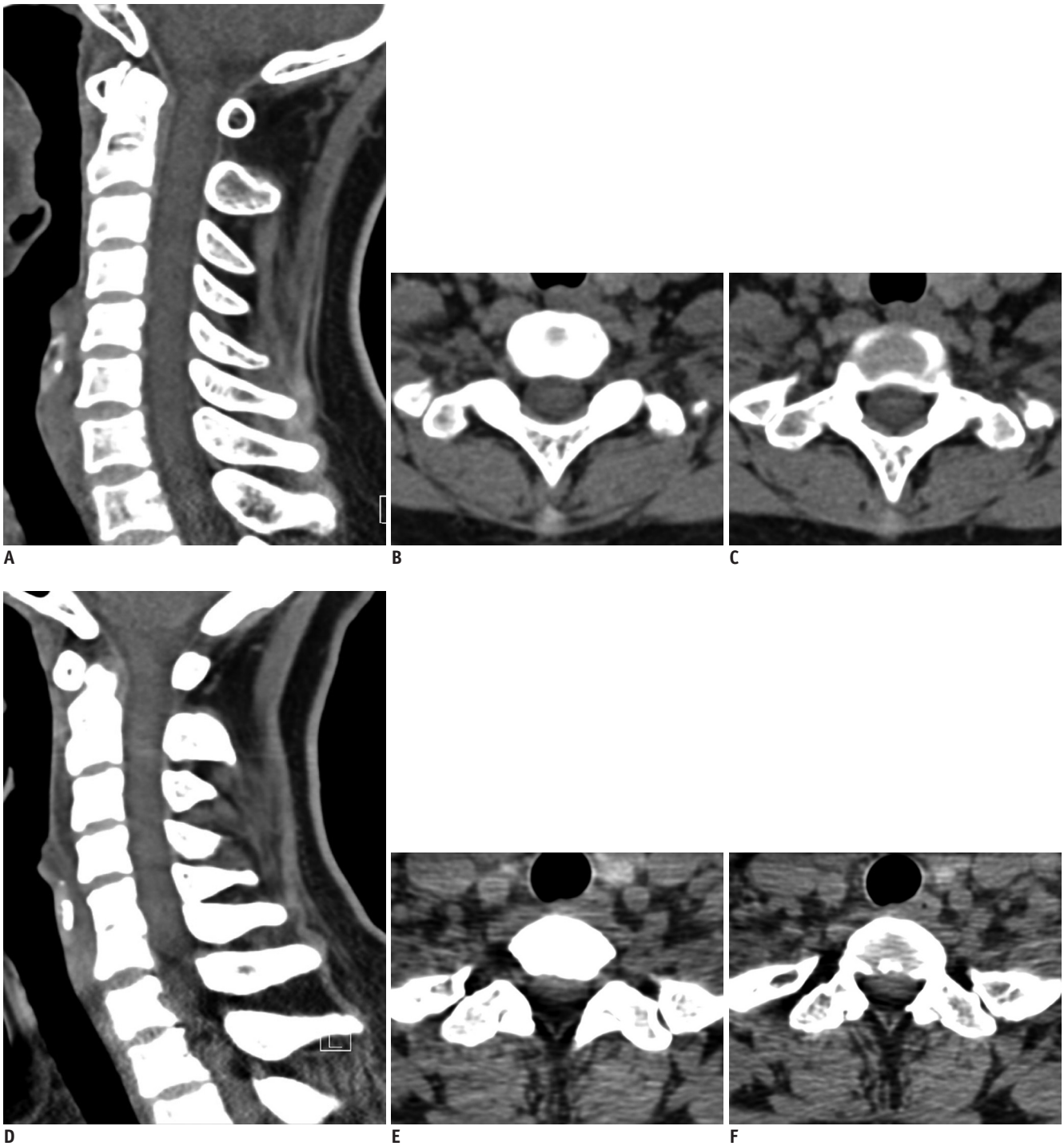

Fig. 4. Comparison of CT images obtained with Sn140-kVp or 120-kVp.
A-C. Cervical spine CT with Sn140-kVp of 49-year-old woman with posterior neck pain (shoulder level, C7; shoulder width, 375 mm; neck diameter, 111 mm). **D-F.** Cervical spine CT with conventional CT with 120-kVp of 43-year-old woman with posterior neck pain (shoulder level, C7; shoulder diameter, 358 mm; neck diameter, 103 mm). **B**, **C**, **E**, and **F** are two consecutive axial images in level of C7/T1. In spite of similar body habitus of shoulder and neck between two patients, artifacts in lower cervical spinal levels are more severe in conventional scan than Sn140-kVp scan. Congenital blocked vertebrae of C5 and C6 is identified in **D**.

https://doi.org/10.3348/kjr.2018.0517

Korean Journal of Radiology
KJR

both Sn140-kV and conventional 120-kVp scans at the C3/4 level where there are no artifacts generated by the shoulder girdles (Table 6). The intermodality agreements for the disc morphology in the lower cervical spinal region were low in both groups; however, the κ values were higher for Sn140-kVp scans than for conventional scans.

Radiation Dose

The $CTDI_{vol}$, DLP, and effective dose were significantly reduced in Sn140-kVp scans than in the conventional 120-kVp scans ($p < 0.001$); all the medians of the radiation doses for Sn140-kVp scans were about 50% less than those for the conventional scans (Fig. 7, Table 7).

In the analysis for the relationship between the body habitus and radiation dose, the radiation dose was significantly positively correlated with the diameters of the shoulders and necks in both Sn140-kVp and the conventional acquisitions, although the coefficients tended to be slightly higher in the conventional CT than in Sn140-kVp scans (Table 8). However, the radiation dose among the shoulder levels of C6, C7, T1, and T2 was not significantly different in both CT scans.

DISCUSSION

Tin is a non-radioactive and non-volatile material. When it is implemented as a filter in the CT tube, it causes spectral shaping of the polychromatic X-ray beam by absorbing the low levels of X-ray energy, which contributes little to the image quality but increases the radiation dose. Hence, a tin filter increases the mean photon energy level and decreases radiation dose exposure to the patients (7, 19). Recently, a tin filter was implemented in a high energy tube in dual-energy DSCT, wherein it increased the

Table 4. Quantitative Image Quality of Cervical Spine CT

	Noise (HU)			Attenuation (HU)		
	Sn140-kVp	120-kVp	*P*	Sn140-kVp	120-kVp	*P*
C3/4	7.4 ± 1.1	7.9 ± 2.6	0.902	29.7 ± 3.6	36.7 ± 5.6	< 0.001
C6/7	10.2 ± 3.2	11.6 ± 4.8	0.286	19.6 ± 12.1	21.6 ± 16.4	0.195
C7/T1	15.4 ± 4.7	22.3 ± 9.0	< 0.001	-2.5 ± 15.5	-19.9 ± 22.7	< 0.001

Data are medians ± interquartile ranges. HU = Hounsfield units

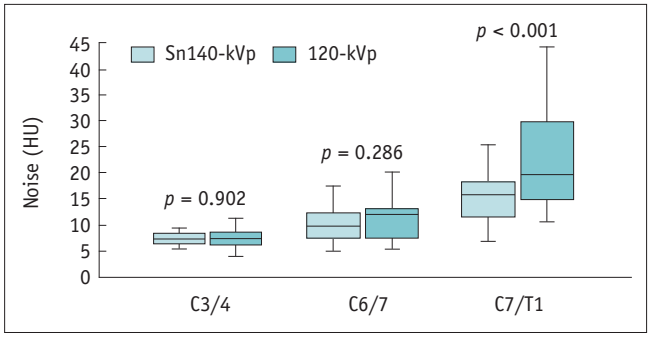

Fig. 5. Box-and-whiskers plots for noise inside central spinal canal. Noise is gradually increased from C3/4 to C7/T1 in both cervical spine CT scans with Sn140-kVp and 120-kVp. At level of C7/T1, noise in Sn140-kVp scans is significantly less than in conventional 120-kVp scans. Boxes represent medians and interquartile ranges and whiskers extend to 1.5 interquartile ranges. HU = Hounsfield units

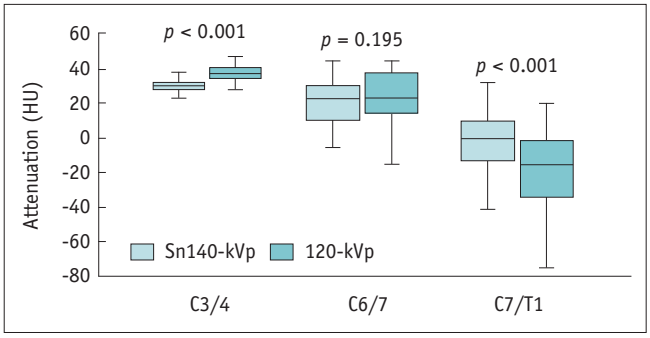

Fig. 6. Box-and-whiskers plots for attenuation values inside central spinal canal. Attenuation gradually decreases from C3/4 to C7/T1 in both cervical spine CT scans with Sn140-kVp and 120-kVp. At level of C7/T1, attenuation in Sn140-kVp scans significantly less decreases than in 120-kVp scans.

Table 5. SNR of Cervical Spinal Bodies and CNR between Spinal Bodies and Central Canal

	SNR_{bone}			$CNR_{bone\text{-}central\ canal}$		
	Sn140-kVp	120-kVp	*P*	Sn140-kVp	120-kVp	*P*
C3	5.3 ± 5.3	5.3 ± 2.1	0.903	4.8 ± 2.2	4.6 ± 1.9	0.867
C6	4.7 ± 1.9	5.0 ± 3.4	0.172	4.2 ± 1.9	4.4 ± 3.2	0.096
C7	5.2 ± 3.4	5.5 ± 2.2	0.328	4.9 ± 3.0	5.4 ± 1.6	0.206

Data are medians ± interquartile ranges. CNR = contrast-to-noise ratios, SNR = signal-to-noise ratios

https://doi.org/10.3348/kjr.2018.0517

energy separation by minimizing the overlap of high and low kVp spectra and improved the material discrimination (19-22). In a study using urinary stone samples, DSCT with a tin filter (80/Sn140-kVp) significantly improved the discrimination between the uric acid containing and non-uric acid containing urinary stones as compared with DSCT without a tin filter (80/140-kVp) (20). In a study about gout protocol CT (22), DSCT using a tin filter (80/Sn150-kVp) had significantly fewer artifacts than DSCT without a tin filter (80/140-kVp).

Since the third-generation of DSCT was introduced in 2014, a tin filter is able to be implemented even in a single energy acquisition (23). Chest CT studies using the third generation DSCT with a single-energy mode and tin filter (Sn100-kVp) showed a reduction in radiation dose and equal to superior image quality in comparison with conventional CT without a tin filer (8-10). In the paranasal sinus and temporal bone CT studies, the CT using a tin filter (Sn100-kVp and Sn150-kVp, respectively) substantially lowered the radiation exposure to patients, while the image quality was preserved (11, 12). Whole body low-dose CT using spectral shaping by a tin filter (Sn100-kVp) in patients with multiple myeloma also showed a sufficient image quality for the depiction of osteolytic lesions, while reducing the radiation dose (13).

Our study demonstrated similar results as these previous studies using a tin filter: the cervical spine CT with Sn140-kVp allowed a significant radiation dose reduction, preserved the image quality in the upper cervical spinal area, and revealed a significantly better image quality

Table 6. Intermodality Agreement for Disc Morphology between Cervical Spine CT and MRI

	Morphology of Disc	
	Sn140-kVp	120-kVp
C3/4	0.824 (0.670–0.978)	0.828 (0.668–0.988)
C5/6	0.760 (0.562–0.957)	0.655 (0.442–0.868)
C6/7	0.658 (0.457–0.858)	0.546 (0.344–0.748)
C7/T1	0.547 (0.247–0.847)	0.124 (-0.162–0.411)

Data are kappas (95% confidence intervals).

Table 7. Radiation Dose of Cervical Spine CT

	Sn140-kVp	120-kVp	*P*
$CTDI_{vol}$ (mGy)	9.8 ± 1.0	19.8 ± 1.8	< 0.001
DLP (mGy·cm)	195.5 ± 27.7	395.0 ± 69.8	< 0.001
Effective dose (mSv)	1.0 ± 0.1	2.0 ± 0.4	< 0.001

Data are medians ± interquartile ranges. $CTDI_{vol}$ = volume CT dose index, DLP = dose length product

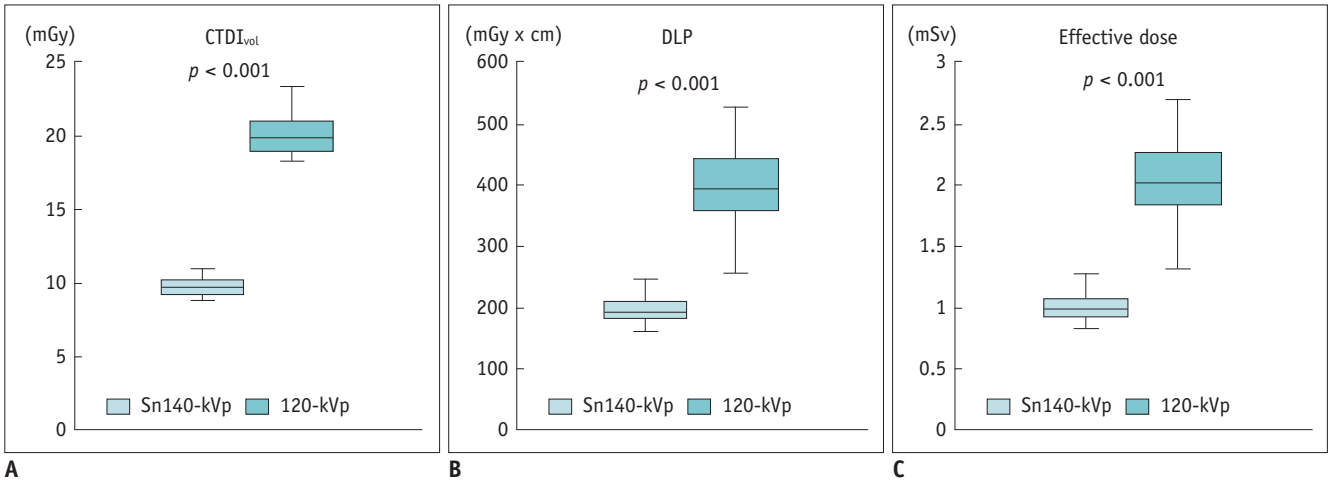

A B C

Fig. 7. Box-and-whiskers plots for radiation dose.
$CTDI_{vol}$ **(A)**, DLP **(B)**, and effective dose **(C)** are significantly reduced in cervical spine CT with Sn140-kVp. $CTDI_{vol}$ = volume CT dose index, DLP = dose length product

Table 8. Relationship between Body Habitus and Radiation Dose

	Sn140-kVp				120-kVp			
	Shoulder RL Diameter		Neck AP Diameter		Shoulder RL Diameter		Neck AP Diameter	
	Coefficient	*P*	Coefficient	*P*	Coefficient	*P*	Coefficient	*P*
$CTDI_{vol}$	0.366	0.043	0.366	0.005	0.620	< 0.001	0.641	< 0.001
DLP	0.450	0.011	0.491	< 0.001	0.721	< 0.001	0.528	< 0.001
Effective dose	0.450	0.011	0.491	< 0.001	0.716	< 0.001	0.512	< 0.001

https://doi.org/10.3348/kjr.2018.0517

Korean Journal of Radiology
KJR

in the lower cervical spine region compared with the conventional CT with 120-kVp. The superior image quality in the lower cervical spinal area for Sn140-kVp acquisitions could be due to the utilization of a high tube voltage, an increased rate of the dose-efficient photons by the tin filter causing a decrease in the energy absorption by the patients and a decrease in the dark band and streak artifacts. The attenuation at the level of C3/4 was significantly lower in Sn140-kVp acquisitions than in the conventional acquisitions. However, it did not affect the intermodality agreement in the assessment of the disc morphology.

A previous study evaluated the intermodality agreement between MRI and CT without the application of the spectral shaping by a tin filter, for herniated discs (24). In that study, the intermodality agreement gradually decreased towards the lower cervical spine level, akin to ours. However, in our study, the intermodality agreement in the lower cervical spinal regions tended to be better in Sn140-kVp scans than that in the conventional scans.

Our study had limitations. First, it was a retrospective study. Thus, the included patients could not undergo both Sn140-kVp and conventional 120-kVp scans. However, the estimated body habitus and demographics that could affect the image quality and radiation dose were not significantly different between the two groups. The parameters between the two protocols were the same except for the use of tin filter, tube voltage, and reference tube current-time products. Second, although information about the patients and protocols was completely removed from a picture archiving and communication system (PACS), we acknowledge that the readers could have recognized the protocols due to the mild difference in the appearance of the images. Third, the intermodality agreement between CT and MRI was assessed only by the disc morphology in spite of many pathologies of the cervical spine. We thought disc herniation was a suitable pathology for this assessment as it was one of the common abnormalities in patients with posterior neck discomfort, and the dark-band and streak artifacts were usually more severe within the central spinal canals. Fourth, although CT is a primary tool for evaluation of fracture, the presence of fractures was not determined. We thought that fracture could affect the image quality due to edema or hemorrhage associated with it and therefore, the cases with fractures were excluded from our study. Instead, the SNR and CNR of the cervical spinal body were calculated. Fifth, iterative reconstruction was not applied in this study. Previous studies demonstrated that iterative reconstruction offered a more noise reduction than filtered back-projection reconstruction (14, 25-27). Thus, a combination of iterative reconstruction and spectral shaping by a tin filter in the cervical spine CT would be more helpful to reduce the artifacts in the lower cervical region.

In conclusion, cervical spine CT with Sn140-kVp decreases artifacts in the lower cervical spinal region, while reducing the radiation exposure in patients, compared with the conventional 120-kVp CT. Thus, a cervical spine CT with Sn140-kVp can be helpful to overcome the artifacts in the lower cervical region.

Conflicts of Interest

The authors have no financial conflicts of interest.

ORCID

Hye Jung Choo
https://orcid.org/0000-0003-3941-6989
Su Min Lee
https://orcid.org/0000-0002-4616-5287

REFERENCES

1. Daffner RH, Hackney DB. ACR Appropriateness Criteria on suspected spine trauma. *J Am Coll Radiol* 2007;4:762-775
2. Douglas-Akinwande AC, Rydberg J, Shah MV, Phillips MD, Caldemeyer KS, Lurito JT, et al. Accuracy of contrast-enhanced MDCT and MRI for identifying the severity and cause of neural foraminal stenosis in cervical radiculopathy: a prospective study. *AJR Am J Roentgenol* 2010;194:55-61
3. Barrett JF, Keat N. Artifacts in CT: recognition and avoidance. *Radiographics* 2004;24:1679-1691
4. Mori I, Machida Y, Osanai M, Iinuma K. Photon starvation artifacts of X-ray CT: their true cause and a solution. *Radiol Phys Technol* 2013;6:130-141
5. Mayo-Smith WW, Hara AK, Mahesh M, Sahani DV, Pavlicek W. How I do it: managing radiation dose in CT. *Radiology* 2014;273:657-672
6. Mueck FG, Roesch S, Geyer L, Scherr M, Seidenbusch M, Stahl R, et al. Emergency CT head and neck imaging: effects of swimmer's position on dose and image quality. *Eur Radiol* 2014;24:969-979
7. Primak AN, Ramirez Giraldo JC, Liu X, Yu L, McCollough CH. Improved dual-energy material discrimination for dual-source CT by means of additional spectral filtration. *Med Phys* 2009;36:1359-1369
8. Braun FM, Johnson TR, Sommer WH, Thierfelder KM, Meinel FG. Chest CT using spectral filtration: radiation dose, image quality, and spectrum of clinical utility. *Eur Radiol* 2015;25:1598-1606

 https://doi.org/10.3348/kjr.2018.0517

9. Gordic S, Morsbach F, Schmidt B, Allmendinger T, Flohr T, Husarik D, et al. Ultralow-dose chest computed tomography for pulmonary nodule detection: first performance evaluation of single energy scanning with spectral shaping. *Invest Radiol* 2014;49:465-473
10. Haubenreisser H, Meyer M, Sudarski S, Allmendinger T, Schoenberg SO, Henzler T. Unenhanced third-generation dual-source chest CT using a tin filter for spectral shaping at 100kVp. *Eur J Radiol* 2015;84:1608-1613
11. May MS, Brand M, Lell MM, Sedlmair M, Allmendinger T, Uder M, et al. Radiation dose reduction in parasinus CT by spectral shaping. *Neuroradiology* 2017;59:169-176
12. Kim CR, Jeon JY. Radiation dose and image conspicuity comparison between conventional 120 kVp and 150 kVp with spectral beam shaping for temporal bone CT. *Eur J Radiol* 2018;102:68-73
13. Suntharalingam S, Mikat C, Wetter A, Guberina N, Salem A, Heil P, et al. Whole-body ultra-low dose CT using spectral shaping for detection of osteolytic lesion in multiple myeloma. *Eur Radiol* 2018;28:2273-2280
14. Becce F, Ben Salah Y, Verdun FR, Vande Berg BC, Lecouvet FE, Meuli R, et al. Computed tomography of the cervical spine: comparison of image quality between a standard-dose and a low-dose protocol using filtered back-projection and iterative reconstruction. *Skeletal Radiol* 2013;42:937-945
15. Lee SH, Lee YH, Suh JS. Accelerating knee MR imaging: compressed sensing in isotropic three-dimensional fast spin-echo sequence. *Magn Reson Imaging* 2018;46:90-97
16. Fardon DF, Williams AL, Dohring EJ, Murtagh FR, Gabriel Rothman SL, Sze GK. Lumbar disc nomenclature: version 2.0: recommendations of the combined task forces of the North American Spine Society, the American Society of Spine Radiology and the American Society of Neuroradiology. *Spine J* 2014;14:2525-2545
17. Deak PD, Smal Y, Kalender WA. Multisection CT protocols: sex- and age-specific conversion factors used to determine effective dose from dose-length product. *Radiology* 2010;257:158-166
18. Landis JR, Koch GG. The measurement of observer agreement for categorical data. *Biometrics* 1977;33:159-174
19. Krauss B, Grant KL, Schmidt BT, Flohr TG. The importance of spectral separation: an assessment of dual-energy spectral separation for quantitative ability and dose efficiency. *Invest Radiol* 2015;50:114-118
20. Stolzmann P, Leschka S, Scheffel H, Rentsch K, Baumüller S, Desbiolles L, et al. Characterization of urinary stones with dual-energy CT: improved differentiation using a tin filter. *Invest Radiol* 2010;45:1-6
21. Wang CK, Tsai JM, Chuang MT, Wang MT, Huang KY, Lin RM. Bone marrow edema in vertebral compression fractures: detection with dual-energy CT. *Radiology* 2013;269:525-533
22. Jeon JY, Lee SW, Jeong YM, Baek HJ. The effect of tube voltage combination on image artefact and radiation dose in dual-source dual-energy CT: comparison between conventional 80/140 kV and 80/150 kV plus tin filter for gout protocol. *Eur Radiol* 2018 Jul 9 [Epub ahead of print]. https://doi.org/10.1007/s00330-018-5622-9
23. Wichmann JL, Hardie AD, Schoepf UJ, Felmly LM, Perry JD, Varga-Szemes A, et al. Single- and dual-energy CT of the abdomen: comparison of radiation dose and image quality of 2nd and 3rd generation dual-source CT. *Eur Radiol* 2017;27:642-650
24. Yi JS, Cha JG, Han JK, Kim HJ. Imaging of herniated discs of the cervical spine: inter-modality differences between 64-slice multidetector CT and 1.5-T MRI. *Korean J Radiol* 2015;16:881-888
25. Iyama Y, Nakaura T, Iyama A, Kidoh M, Katahira K, Oda S, et al. Feasibility of iterative model reconstruction for unenhanced lumbar CT. *Radiology* 2017;284:153-160
26. Notohamiprodjo S, Stahl R, Braunagel M, Kazmierczak PM, Thierfelder KM, Treitl KM, et al. Diagnostic accuracy of contemporary multidetector computed tomography (MDCT) for the detection of lumbar disc herniation. *Eur Radiol* 2017;27:3443-3451
27. Costello JE, Cecava ND, Tucker JE, Bau JL. CT radiation dose: current controversies and dose reduction strategies. *AJR Am J Roentgenol* 2013;201:1283-1290

https://doi.org/10.3348/kjr.2018.0517